Figure 5.   Attenuation α of moist air (u = 100%) for frequencies below 1000 GHz at sea-level (p = 1013 mb) and temperatures ± 40°C: —— MPM93, ···· Continuum.

Complex permittivity of pure water is expressed by a double-Debye model,[22]

$$\epsilon_w = \epsilon_o - \nu \left[(\epsilon_o - \epsilon_1)/(\nu + i\,\gamma_1) + (\epsilon_1 - \epsilon_2)/(\nu + i\,\gamma_2) \right], \quad (9)$$

which provided a best fit to measured ϵ_w data. The static and high-frequency permittivities are

$$\epsilon_o = 77.66 + 103.3\,(\theta - 1),$$

$$\epsilon_1 = 0.0671\,\epsilon_o, \qquad \epsilon_2 = 3.52 ;$$

and the two relaxation frequencies are

$$\gamma_1 = 20.20 - 146\,(\theta - 1) + 316\,(\theta - 1)^2,$$

$$\gamma_2 = 39.8\,\gamma_1 \quad \text{GHz.}$$

The slight temperature dependence of ϵ_2 (reported in Ref. 22) was eliminated to avoid nonphysical behavior for supercooled (-20 to -40°C) water at frequencies above 100 GHz.

A permittivity model for ice was reported by Hufford,[23]

$$\epsilon_i = 3.15 + i\,(a_i/\nu + b_i\,\nu), \quad (10)$$

where

$$a_i = (\theta - 0.171)\exp(17.0 - 22.1\,\theta)$$

and

$$b_i = \left\{ [0.233/(1 - 0.993/\theta)]^2 + 6.33/\theta - 1.31 \right\} 10^{-5}.$$

The MPM for fog/cloud cases is $N = N_D + N_V + N_W$. Related attenuation (α) and delay (τ) rates up to 120 GHz are plotted in Fig. 6 for a normalized mass density, w = 1 g/m³ (heavy fog, about 50 m visibility) suspended in saturated, sea-level air (± 30°C). Below freezing, liquid properties were changed to those of ice. Above freezing one notices that the combined attenuation is almost independent of temperature.

3.   RADIO-PATH CHARACTERISTICS

The electromagnetic spectrum between 100 and 1000 GHz is available to expand radio services. This band offers favorable alternatives to both microwave and ir/optical systems. Applications in communication, radar, and remote sensing can profit from larger bandwidth, smaller antenna sizes for a given spatial resolution, high frequency resolution and, in contrast to ir/optical ranges, a favorable performance under fog/cloud conditions. Besides technical difficulties, the attenuating nature of the earth's atmosphere seriously limits usable path lengths. Except for a few window ranges, the medium at ground levels (h ≤ 1 km) is opaque due to strong absorption lines of water vapor. High mountain sites (h ≤ 4 km), airplanes (h ≤ 15 km), and balloons (h ≤ 35 km) are alternative platforms to escape the water-vapor limitations.

A predictive broadband (1 - 1000 GHz) model for radio characteristics of the neutral atmosphere (h ≤ 130 km) was developed to allow prompt evaluations of the highly variable propagation effects from basic data. Performance of established applications (≤ 30 GHz) can be translated to (frequency scaling) or combined with new schemes and economical assessments of feasible trade-offs and adaptive measures can be made.

3.1   Transmission and Emission Formulations

Propagation through the nonscattering and nonturbulent inhomogeneous atmosphere is described by the line integral $\int N\,ds$, where ds is a path differential and the refractivity N was discussed in Sect. 2. Height profiles of N are the basis for calculating delay and loss along the path. Excess delay,

$$D = 3.3356 \int (N_o + N')ds \quad \text{ps,}$$

is linked to the real part and total path attenuation,

$$A = 0.1820\,\nu \int N''\,ds \quad \text{dB,} \quad (11)$$

to the imaginary part.[26] The transmission factor,

$$\Gamma = 10^{-0.1\,A}, \quad (12)$$

evaluates the energy transfer. A path is said to be opaque when less than 0.1% of the original energy is passed ($\Gamma \leq 0.001$, $A \geq 30$ dB). The absorbing atmosphere maintains, up to approximately 90 km height, thermal equilibrium and emits noise radiation at the equivalent blackbody temperature,

$$T_B = 4.191 \times 10^{-2}\,\nu \int T(s)\,N''(s)\,\Gamma(s_o,s)\,ds \quad \text{K.} \quad (13)$$

Decreasing transmission leads to increasing emission. The weighting function,

$$W(s) = 4.191 \times 10^{-2}\,\nu\,N''(s)\,\Gamma(s_o,s), \quad (14)$$

determines the height range from where the emission originates. Two cases can be made based on the integration limits for A. In the first one, A is evaluated "upwards", starting at the initial height, h_o; secondly, the start is at the final height, h_∞, and moves "downwards". Reciprocity between path attenuation A_i and brightness $T_{B,i}$ was assumed for polarization-sensitive computations based on the matrix $\mathbf{N}$.

3.2   Atmospheric Radio-Path Model

The MPM code (see Sect. 2) is applied in a radio-path model which simulates propagation through an inhomogeneous medium. The atmosphere is spherically stratified in concentric layers between h = 0 and 130 km separated by 1-km increments (Δh). Values for N(h) are enumerated by height profiles of p(h), t(h), and u(h). The U.S. Standard Atmosphere and the mid-latitude mean water-vapor profile[24] are the defaults of the path model. All computed examples given below are for the default case. It is not difficult to implement different model atmospheres or radiosonde data.
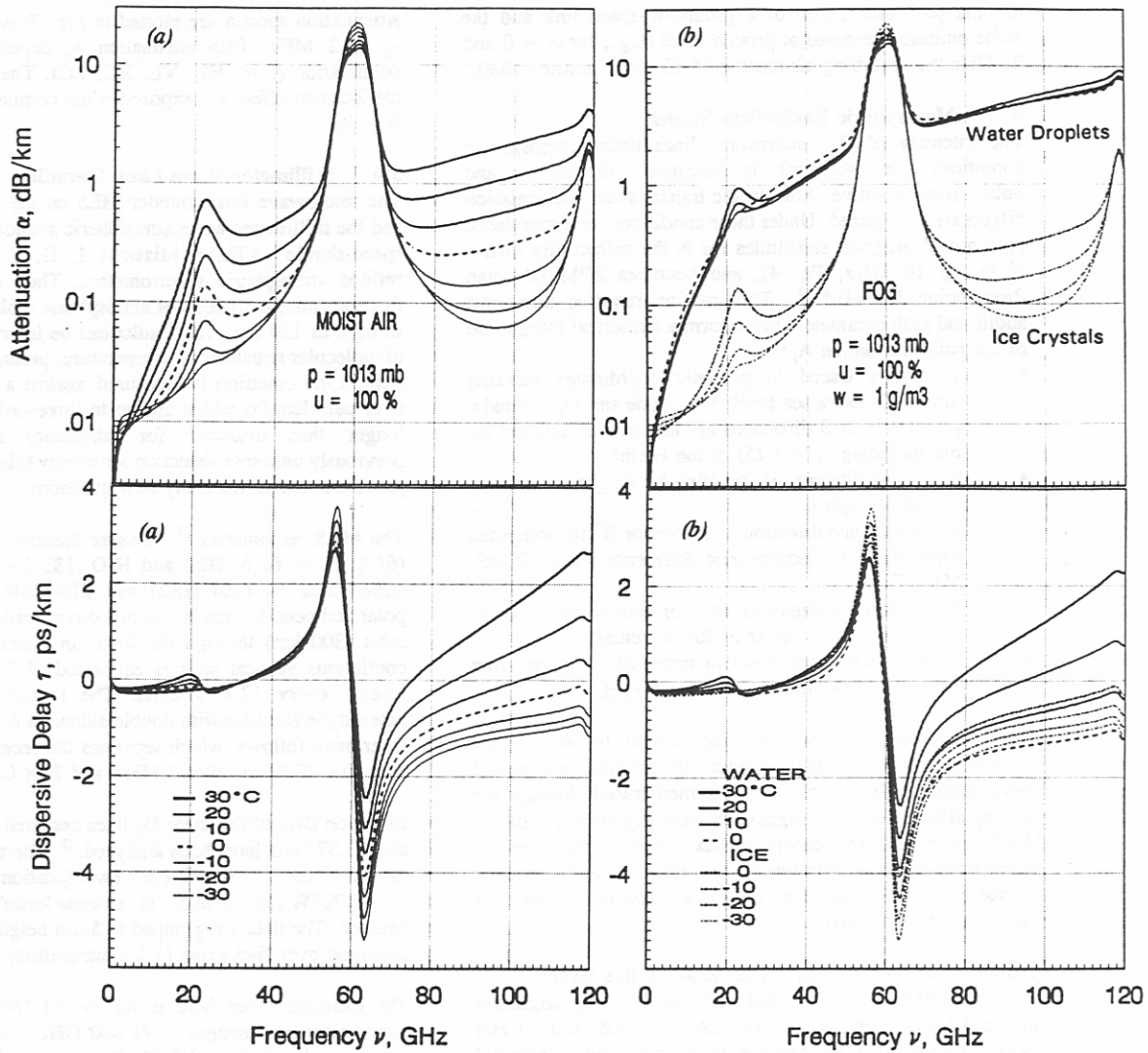
Figure 6.   Attenuation rate $\alpha(\nu)$ and delay rate $\tau(\nu)$ up to 120 GHz at temperatures $\pm 30\,°C$:
(a) Moist air at sea-level, $u = 100\,\%$,   (b) water droplets or ice crystals, $w = 1\ g/m^3$, added to (a).

The path differential ds of a slant path is computed by means of the rules of spherical geometry. For elevation angles, $\varphi \geq 10°$, the secant law $ds = \Delta h/\sin \varphi$ follows. In fact, both the curvature of the Earth and refraction determine the path extension of Δh. At very low elevation angles ($\varphi \rightarrow 0$), the height interval Δh is subdivided into 10×0.1-km and further, if needed, into 10×0.01-km groups to approximate more nearly a continuum of N values. When a maximum change of $A_h - A_{h-1} \geq 0.1$ dB is detected across an integration layer, the linear interpolation initiates automatically.

The numerical integration of A (Eq. 11) stops at heights h_∞ when increments ΔA become smaller than 0.01 dB (for a limb path after advancing past the tangential height). The path length L is that between h_o and h_∞. A numerical integration of T_B (Eq. 13) for emission radiating to the height h_o follows

$$T_B \approx 0.2303 \sum_h [T(h)(A_h - A_{h-1})\ \Gamma(h)] + 2.7\ \Gamma(\infty), \quad (15)$$

where $2.7\ \Gamma(\infty)$ is the cosmic background term. Superfluous computations are stopped when $W(h) \leq 10^{-6}$. The radio-path model operates at any frequency between 1 and 1000 GHz, and Table 3 summarizes results for 21 and 45 GHz. Listed

TABLE 3.
Total Attenuation A and Emission T_B at 21 and 45 GHz
Through a Model Atmosphere.[24]

Surface values at h_o: 1013 mb, 15°C, $q = 3.57\ g/m^3$
($\int q(h)dh = 10.6$ mm for zenith, $\varphi = 90°$)

ν	A	T_B	φ	h_∞	L
GHz	dB	K	deg	km	km
21.0	0.28	19.2	90	11	11
	0.56	34.9	30	13	26
	0.82	48.5	20	15	44
	1.60	85.1	10	17	94
	15.7	274.4	0	26	577
45.0	0.66	39.2	90	17	17
	1.32	71.1	30	19	38
	1.93	96.4	20	22	64
	3.74	154.9	10	21	115
	32.0	285.6	0	31	650

are the path attenuation of a ground-to-space link and the noise emission received at ground level (e.g., for $\varphi = 0$ and 21 GHz the absorbing air mass is 56 times the zenith value).

3.3 Mesospheric Radio-Path Model

The intensity of O_2 microwave lines under mesospheric conditions ($\geq$ 40 km) is location-, direction-, and polarization-sensitive. Anisotropic transmission and emission effects are recognized. Under these conditions the atmospheric path model program substitutes for N the refractivity matrix $\bar{\mathbb{N}}$ ($\nu_k \pm 10$ MHz, Eq. 4), and becomes ZPM (Zeeman Propagation Model).[8, 9] This routine requires numerous additional path parameters to perform a numerical integration of the path attenuation A_i:

- A ray is traced in geodetic coordinates marking altitude h above sea level, LA_titude and LO_ngitude [heights in N-S directions are adjusted to account for the flattening (1/298.25) of the Earth]
- The wave direction is specified by AZ_imuth and elevation angle φ
- Magnitude and direction of the vector B^* are computed using the Int. Geomagnetic Reference Field (IGRF-MAGFIN)[25]
- Polarization of launched wave or emitted noise power is selected (H/V-Linear or R/L-Circular)
- A frequency range is set in terms of deviation from the selected O_2 line center ($\Delta\nu = \nu_k \pm \nu$).

Two characteristic waves are represented by normalized Stokes parameters and combined to produce the initial polarization.[8] This combination is then traced through the propagation distance L. Eigenvalues and eigenvectors of the 2×2 plane-wave refractivity matrix are calculated for the orientation angle ϕ between wave vector E^* and magnetic vector B^*. The propagating field is a linear combination of two characteristic waves.

Individual integration steps of ZPM at the line center, $\nu_k = 61.150$ GHz, are detailed in Table 4: A ray originates at the 300-km orbital height (h, LA, LO, AZ, and φ) and passes through the atmosphere to a minimum, tangential height, $h_t = 90$ km.

Attenuation spectra are plotted in Fig. 7 over the range, $\nu_k \pm 2$ MHz. Path attenuation A_i depends on the initial polarization (i = HL, VL, RC, LC). The main features of the Zeeman effect are exposed when compared with the case B = 0.

3.4 Millimeter-Wave Limb Sounding

The microwave limb sounder MLS on the UARS satellite[26] and the millimeter-wave atmospheric sounder MAS[27] on the space-shuttle (ATLAS Missions I, II, ...) both are very refined atmospheric spectrometers. They measure globally thermal emission spectra of atmospheric molecules at altitudes as high as 150 km. The results can be interpreted in profiles of molecular abundances, temperature, pressure, and magnetic field. Line emission is measured against a 3 K background over path lengths which are up to three-orders of magnitude longer than available for laboratory spectroscopy. A previously unknown detection sensitivity brings answers to old problems and raises many new questions.

The MAS radiometers[27] measure thermal emission from O_2 (61.1, 63.0, 63.6 GHz) and H_2O (183 GHz), and from the trace gases O_3 (184 GHz) and ClO (204 GHz). An HL-polarized pencil-beam is scanned downwards from the shuttle orbit (300 km) through the limb. In normal operation, the continuous vertical scan is calibrated (2.7 and 300 K) and repeats every 12.8 seconds. The radiometers are super-heterodyne receivers with double-sideband (DSB) detection. A filter bank follows, which separates the received noise power into $10\times$ 40-MHz, $20\times$ 2-MHz, and $20\times$ 0.2-MHz outputs.

Emission data of the three O_2 lines centered at 61.15, 63.00, and 63.57 GHz have been analyzed.[28] The tangential heights ranged from 125 to 10 km. Two locations were selected: 70°N, 70°W (shuttle at 57°N, antenna looks north) and at the equator. The data are grouped in 5-km height increments and averaged over five scans (1.2 s integration).

The example given here is for the 61.150 GHz line. The upper sideband (image) at 71.630 GHz responds to cosmic background radiation (2.7 K). The measured mean is to first order about half the theoretical single sideband level.

TABLE 4.

Path Attenuation $A_i(h)$ and Noise Emission $T_{B,i}$ for a Limb Path ($h_t = 90$ km) at $\nu_0 = 61.15056$ GHz. Antenna is located at 57°N/70°W, h = 300 km and looks down ($\varphi = -14.57°$) towards north (AZ = 0°) to receive linear-polarized radiation (results for i = VL-, RC- and LC-polarizations are also given).

| h	LA	LO	AZ	φ	B	ϕ	L	A_{HL}	A_{VL}	W_{HL}	W_{VL}	A_{RC}	A_{LC}
km	deg	deg	deg	deg	μT	deg	km	dB		km^{-1}		dB	
300	57.0	-70	0	-14.57			0	T_B(DBS) =		67.8 K (ZPM)		63$\pm$2 K (MAS)	
$\downarrow$							$\downarrow$	T_B(SSB) =		131.2	174.5	153.0	153.0 K
129	65.2	-70	0	-6.39	55.1	78.4	954	0.00	0.00	.000	.000	0.00	0.00
$\downarrow$							$\downarrow$			$\uparrow$			
91	70.4	-70	0	-1.14	55.4	85.6	1548	1.30	2.92	.060	.094	2.03	2.03
90	71.0	-70	0	-0.53	55.4	86.2	1616	1.97	4.45	.099	.126	3.04	3.04
91	72.1	-70	0	0.53	55.3	87.3	1736	3.39	7.66	.150	.127	5.02	5.02
92	72.7	-70	0	1.14	55.2	88.4	1805	4.06	9.20	.061	.042	5.91	5.91
$\downarrow$							$\downarrow$						
129	77.7	-70	0	6.15	53.7	94.9	2371	5.15	11.68	.000	.000	7.29	7.29
130	77.8	-70	0	6.23	53.7	95.0	2380	5.15	11.68	.000	.000	7.29	7.29
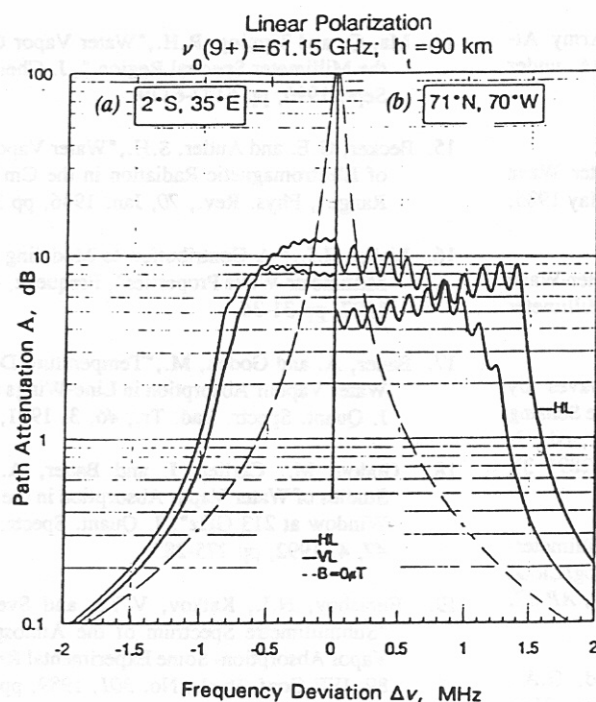
Figure 7. Spectra ($\nu_o \pm 2$ MHz) of total attenuations A_i ($i = $ HL, VL) and A_o (B = 0) for a limb path ($h_t = 90$km) through the U.S. Std. Atm. [24] at two locations marked (a) and (b).

The data are shown in Fig. 8 and serve as a test case for ZPM predictions.[24, 25] Limb-emission was measured for tangential heights ranging from 30 to 120 km at the northern location 71°N/70°W. Table 4 lists the variables that enter a computation of $T_B(\nu_k)$. Very height-selective ($\Delta h \leq 1$ km) temperature sounding between 115 and 80 km is indicated by the weighting function W(h), Eq. (14). At $h_t = 78$ km, the path abruptly becomes opaque and T_B assumes about half the physical temperature of the 78-km level (98 K). Below $h_t = 40$ km, the upper sideband at 71.63 GHz "warms up" due to absorption by water vapor and dry air, which is computed by means of MPM.

4. CONCLUSIONS

Propagation characteristics of the atmosphere are predicted by the general refractivity N, and for Zeeman-broadening by the special refractivity matrix $\mathbb{N}$. Transmission and emission properties of the inhomogeneous atmosphere (e.g., excess path delay, total attenuation, opacity, sky noise, etc.) were modeled from known path profiles of physical variables.

The new code MPM93 reproduces the spectral characteristics of the clear atmosphere (O_2, H_2O) between 18 and 930 GHz within the uncertainty limits of five reported controlled experiments.[15 - 19]

ZPM reproduces the main features of measured thermal radiation signatures stemming from Zeeman-split oxygen lines. The solution to the forward-transfer problem [8, 9, 28] can serve as a starting point to develop profile inversion algorithms.[7, 13] Validation, error checking of predictions, and incorporation of new research results will continue to be critical and time consuming tasks in the effort to refine understanding and modeling of electromagnetic wave propagation through the neutral atmosphere.
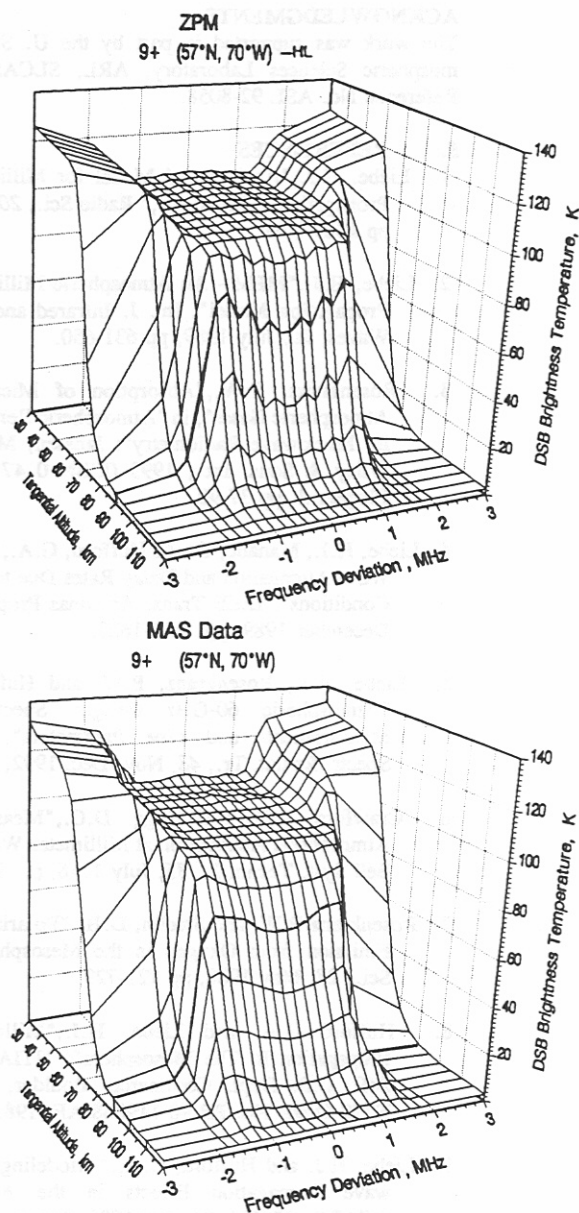

Figure 8. DSB-emission of the 9^+ line ($\nu_k \pm 3$ MHz) from a limb scan, $h_t = 30$ to 120 km, approximatly centered over 70°N, 70°W: (a) ZPM predictions for HL polarization and (b) MAS data[**].

5.   REFERENCES

1.   Liebe, H.J., "An Updated Model for Millimeter Wave Propagation in Moist Air," Radio Sci., 20, May 1985, pp 1069-1089.

2.   Liebe, H.J., "MPM - An Atmospheric Millimeter-Wave Propagation Model", Int. J. Infrared and Millimeter Waves, 10, July 1989, pp 631-650.

3.   Rosenkranz, P.W., "Absorption of Microwaves by Atmospheric Gases", in "Atmospheric Remote Sensing By Microwave Radiometry"; Janssen, M.A., ed.; J. Wiley & Sons, Inc., 1993 (ISBN 0 471 62891 3), Chapter 2, pp 37-90.

4.   Liebe, H.J., Manabe, T. and Hufford, G.A., "Millimeter-Wave Attenuation and Delay Rates Due to Fog/Cloud Conditions", IEEE Trans. Antennas Propag., AP-37, December 1989, pp 1617-1623.

5.   Liebe, H.J., Rosenkranz, P.W. and Hufford, G.A., "Atmospheric 60-GHz Oxygen Spectrum: New Measurements and Line Parameters", J. Quant. Spectr. Radiat. Tr., 48, Nov./Dec. 1992, pp 629-643.

6.   Crawford, A.B. and Hogg, D.C., "Measurement of Atmospheric Attenuation at Millimeter Wavelengths", Bell Syst. Techn. J., 35, July 1956, pp. 907-916.

7.   Rosenkranz P.W. and Staelin, D.H., "Polarized Thermal Emission from Oxygen in the Mesosphere", Radio Sci., 23, May 1988, pp 721-729.

8.   Hufford G.A. and Liebe, H.J., "Millimeter-Wave Propagation In The Mesosphere", NTIA-Report 89-249, U.S. Dept. Commerce, Boulder, CO, 1989; NTIS Order No. PB 90-119868/AF (1989).

9.   Liebe, H.J. and Hufford, G.A., " Modeling Millimeter-wave Propagation Effects in the Atmosphere", AGARD CP-454, October 1989, Paper 18.

10. Goff, J.A. and Gratch, S., "Low-Pressure Properties of Water from -160 to 212°F", Trans. Amer. Soc. Heat. Vent. Eng., 52, 1946, pp 95-121 (also see List, R.J., "Smithonian Meteorological Tables", Washington D.C., Smithonian Inst., 1966).

11. Bauer, A., Godon, M., Kheddar, M. and Hartmann, J.M., "Temperature and Perturber Dependences of Water Vapor Line-Broadening: Experiments at 183 GHz, Calculations Below 1000 GHz", J. Quant. Spectr. Radiat. Tr., 41, 1, 1989, pp 49-54.

12. Poynter, R.L., Pickett, H.M., and Cohen, E., "Submillimeter, Millimeter, and Microwave Spectral Line Catalogue", JPL Publication 80-23, Revision 3, 1991, NASA-JPL, Pasadena, CA.

13. Westwater, Ed.R., "Groundbased Microwave Radiometry", in "Atmospheric Remote Sensing By Microwave Radiometry", Janssen, M.A., ed.; J. Wiley & Sons, Inc., 1993 (ISBN 0 4710 62891 3), pp 145-213.

14. Ma, Q. and Tipping, R.H., "Water Vapor Continuum in the Millimeter Spectral Region ", J. Chem. Phys., 93, Sept. 1990, pp 6127-6139.

15. Becker, G.E. and Autler, S.H., "Water Vapor Absorption of Electromagnetic Radiation in the Cm Wave-length Range", Phys. Rev., 70, Jan. 1946, pp 300-307.

16. Liebe, H.J., " A Contribution to Modeling Atmospheric Millimeter-Wave Properties", Frequenz, 41, Jan./Feb. 1987, pp 31-36.

17. Bauer, A. and Godon, M., "Temperature Dependence of Water Vapour Absorption in Line-Wings at 190 GHz", J. Quant. Spectr. Rad. Tr., 46, 3, 1991, pp 211-220.

18. Godon, M., Carlier, J. and Bauer, A., "Laboratory Studies of Water Vapor Absorption in the Atmospheric Window at 213 GHz", J. Quant. Spectr. Radiat. Tr., 47, 4, 1992, pp 275-285.

19. Furashov, N.I., Katkov, V.Yu. and Svertlov, B.A., "Submillimetre Spectrum of the Atmospheric Water Vapor Absorption- Some Experimental Results", ICAP 89, IEE Conf. Publ., No. 301, 1989, pp 310-311.

20. Hill, R.J., "Dispersion by Atmospheric Water Vapor at Frequencies Less Than 1 THz", IEEE Trans. Antennas Propag., AP-36, 3, March 1988, pp 423-430.

21. Rosenkranz, P.W., "Pressure Broadening of Rotational Bands.II. Water Vapor from 300 to 1100 cm^{-1} ", J. Chem. Phys., 87, July 1987, pp 163-170.

22. Liebe, H.J., Hufford, G.A. and Manabe, T., "A Model for the Complex Permittivity of Water at Frequencies Below 1 THz", Int. J. Infrared and Millimeter Waves, 12, July 1991, pp 659-675.

23. Hufford, G.A., "A Model for the Complex Permittivity of Ice at Frequencies Below 1 THz", Int. J. Infrared and Millimeter Waves, 12, July 1991, pp 677-680.

24. COESA, U.S. Committee on Extension to the Standard Atmosphere, "U.S. Standard Atmosphere 76", NOAA-S/T 76-1562; U.S. Gov. Printing Office, Washington, D.C., 1976.

25. Barraclough, D.R., "International Geomagnetic Reference Field revision 1985", Pure and Appl. Geophys., 123, 1985, pp 641-645.

26. Waters, J.W., "Microwave Limb Sounding", in "Atmospheric Remote Sensing By Microwave Radiometry", Janssen, M.A., ed.; J. Wiley & Sons, Inc., 1993 (ISBN 0 4710 62891 3), Chapter 8, pp 383-496.

27. Croskey, C.L. et al., "The Millimeter Wave Atmospheric Sounder (MAS): A Shuttle-Based Remote Sensing Experiment", IEEE Trans. Microw. Theory and Techniques, MTT-40, June 1992, pp 1090-1099.

28. Cotton, M.G., Degenhardt, W., Hartmann, G.K., Hufford, G.A., Liebe, H.J., and Zwick, R., "Analysis of MAS Emission Signatures from three O_2 Microwave Lines", NTIA Report 93-000, in review, 1993.

**DISTRIBUTION OF UNCLASSIFIED
AGARD PUBLICATIONS**

AGARD holds limited quantities of the publications that accompanied Lecture Series and Special Courses held in 1993 or later, and of AGARDographs and Working Group reports published from 1993 onward. For details, write or send a telefax to the address given above. *Please do not telephone.*

AGARD does not hold stocks of publications that accompanied earlier Lecture Series or Courses or of any other publications. Initial distribution of all AGARD publications is made to NATO nations through the National Distribution Centres listed below. Further copies are sometimes available from these centres (except in the United States). If you have a need to receive all AGARD publications, or just those relating to one or more specific AGARD Panels, they may be willing to include you (or your organisation) on their distribution list. AGARD publications may be purchased from the Sales Agencies listed below, in photocopy or microfiche form.

NATIONAL DISTRIBUTION CENTRES

BELGIUM
Coordonnateur AGARD — VSL
Etat-Major de la Force Aérienne
Quartier Reine Elisabeth
Rue d'Evere, 1140 Bruxelles

CANADA
Director Scientific Information Services
Dept of National Defence
Ottawa, Ontario K1A 0K2

DENMARK
Danish Defence Research Establishment
Ryvangs Allé 1
P.O. Box 2715
DK-2100 Copenhagen Ø

FRANCE
O.N.E.R.A. (Direction)
29 Avenue de la Division Leclerc
92322 Châtillon Cedex

GERMANY
Fachinformationszentrum
Karlsruhe
D-7514 Eggenstein-Leopoldshafen 2

GREECE
Hellenic Air Force
Air War College
Scientific and Technical Library
Dekelia Air Force Base
Dekelia, Athens TGA 1010

ICELAND
Director of Aviation
c/o Flugrad
Reykjavik

ITALY
Aeronautica Militare
Ufficio del Delegato Nazionale all'AGARD
Aeroporto Pratica di Mare
00040 Pomezia (Roma)

LUXEMBOURG
See Belgium

NETHERLANDS
Netherlands Delegation to AGARD
National Aerospace Laboratory, NLR
P.O. Box 90502
1006 BM Amsterdam

NORWAY
Norwegian Defence Research Establishment
Attn: Biblioteket
P.O. Box 25
N-2007 Kjeller

PORTUGAL
Força Aérea Portuguesa
Centro de Documentação e Informação
Alfragide
2700 Amadora

SPAIN
INTA (AGARD Publications)
Pintor Rosales 34
28008 Madrid

TURKEY
Milli Savunma Başkanlığı (MSB)
ARGE Daire Başkanlığı (ARGE)
Ankara

UNITED KINGDOM
Defence Research Information Centre
Kentigern House
65 Brown Street
Glasgow G2 8EX

UNITED STATES
National Aeronautics and Space Administration (NASA)
Langley Research Center
M/S 180
Hampton, Virginia 23665

The United States National Distribution Centre (NASA/Langley) does NOT hold stocks of AGARD publications.
Applications for copies should be made direct to the NASA Center for Aerospace Information (CASI) at the address below.

SALES AGENCIES

NASA Center for
  Aerospace Information (CASI)
800 Elkridge Landing Road
Linthicum Heights, MD 21090-2934
United States

ESA/Information Retrieval Service
European Space Agency
10, rue Mario Nikis
75015 Paris
France

The British Library
Document Supply Centre
Boston Spa, Wetherby
West Yorkshire LS23 7BQ
United Kingdom

Requests for microfiches or photocopies of AGARD documents (including requests to CASI) should include the word 'AGARD' and the AGARD serial number (for example AGARD-AG-315). Collateral information such as title and publication date is desirable. Note that AGARD Reports and Advisory Reports should be specified as AGARD-R-nnn and AGARD-AR-nnn, respectively. Full bibliographical references and abstracts of AGARD publications are given in the following journals:

Scientific and Technical Aerospace Reports (STAR)
published by NASA Scientific and Technical
Information Program
NASA Headquarters (JTT)
Washington D.C. 20546
United States

Government Reports Announcements and Index (GRA&I)
published by the National Technical Information Service
Springfield
Virginia 22161
United States
(also available online in the NTIS Bibliographic
Database or on CD-ROM)